

Supporting information for:

Design Principles of Perovskites for Solar-Driven Thermochemical Splitting of CO₂

M. Ezbiria, M. Takacs^a, B. Stolza, J. Lunghok, A. Steinfeld^a, R. Michalsky^{a,*}

^a Department of Mechanical and Process Engineering, ETH Zürich, 8092 Zürich, Switzerland

Overview Supporting Information

1. Computational details

- a. Structure optimizations
- b. Free energy computations
- c. Scaling relations
- d. Stability computations

2. Supporting data

- a. Experimental data
 - i. XRD of CeCoO₃
 - ii. XRDs of as-prepared perovskites to be tested via TGA
 - iii. Oxygen nonstoichiometry
 - iv. TGA
 - v. HT-XRD for material stability
 - vi. RT-XRD
 - vii. TEM
- b. Thermochemical equilibrium analysis

3. References

1. Computational details

a. Structure optimizations

Both, ASE and GPAW are open-source codes available from the Department of Physics at the Technical University of Denmark and are available at <https://wiki.fysik.dtu.dk/ase/> and <https://wiki.fysik.dtu.dk/gpaw/>.

Table S1: Minimum and maximum values of calculated lattice constants (a) and magnetic moments of the transition metals (M) at the B sites of cubic (space group 221) AB₃, AA'BO₃, ABB'O₃ and AA'BB'O₃ perovskites.

Type of perovskite	a (Å)	M(B) (μ_B)	M(B') (μ_B)
ABO ₃	3.7357 – 4.2914	0.2453 – 3.8368	
AA'BO ₃	3.7953 – 4.2000	0.2757 – 3.7985	0.2760 – 3.8000
ABB'O ₃	3.6000 – 4.1419	0.0040 – 4.2172	-3.1064 – 3.8337
AA'BB'O ₃	3.7998 – 4.1274	-2.2340 – 3.880	-2.3856 – 3.5935

The DFT-computed lattice constants compare well, within the uncertainty of DFT calculations¹⁻², with the experimental values for cubic perovskites of similar composition. For example, the relative error is 1.06% when comparing DFT-computed 3.9566 Å (La_{0.5}Sr_{0.5}MnO₃) to an experimental value of 3.915 Å (La_{0.67}Sr_{0.33}MnO₃)³ or 0.07-1.38% when comparing DFT-computed 3.9276 Å (La_{0.5}Sr_{0.5}Fe_{0.5}Co_{0.5}O₃) to experimental values of about 3.925 Å (La_{0.6}Sr_{0.4}Co_{0.2}Fe_{0.8}O_{3-δ})⁴ and 3.874 Å (La_{0.6}Sr_{0.4}Co_{0.2}Fe_{0.8}O₃)⁵ or 2.17% when comparing 3.9183 Å (SrCoO₃) to an experimental value of 3.835 Å (SrCoO₃)⁶.

b. Free energy computations

Free energies of the chemical species *i* (G_i) were calculated via:¹

$$G_i(T, P) = N_i \mu_i(T, P) = E_i + U_{ZPE,i} - TS_i(T, P) \quad (1)$$

where *T* and *P* are the absolute temperature (298.15 K) and pressure (1.013 bar), *N_i* is the number of atoms, μ_i is the chemical potential, E_i is the total electronic energy determined from DFT-based structure optimization, $U_{ZPE,i}$ is the zero-point vibrational energy, and S_i is the entropy. Gases are assumed to be ideal, while liberated lattice oxygen is treated using the harmonic approximation where all degrees of freedom are treated as frustrated harmonic vibrations and pressure-volume contributions are neglected. Thermodynamic properties were calculated from vibrational frequencies and standard statistical mechanical equations evaluated through ASE. Free energy corrections of the solids are neglected.⁷

Analogously, the enthalpy of forming oxygen vacancies ($\Delta H_v[O]$) at the surface is defined as:

$$\Delta H_v[O] = \Delta G_v[O] + T\Delta S_v[O] \quad (2)$$

where $\Delta S_v[O]$ is the entropy of forming oxygen vacancies.

Free energies and enthalpies are relative to the chemical potential of stable H_2O and H_2 gas, that is, E_O^r is given with:¹

$$E_O^r = E[H_2O] - E[H_2] \quad (3)$$

where $E[H_2O]$ and $E[H_2]$ are the total electronic energy of reference H_2O and H_2 molecules in the gas phase.

c. Scaling relations

Eq. (5) in the main text is based on data for TiO_2 (rutile), Ti_2O_3 , Cu_2O , ZnO (wurtzite), MoO_3 , Ag_2O , $Ba_{0.5}Sr_{0.5}Co_{0.5}Fe_{0.5}$ (cubic), and $La_{0.5}Sr_{0.5}Co_{0.5}Fe_{0.5}$ (cubic). Data for cubic ZrO_2 , cubic $Y_2Zr_6O_{15}$, Y_2O_3 -stabilized ZrO_2 , CeO_2 , and $La_{0.67}Sr_{0.33}MnO_3$ was disregarded due to a large deviation of oxygen nonstoichiometry (δ) between the thermochemical data for bulk metal oxides and the DFT data for metal oxide surfaces.⁸ Differences of factor 16-32 for the nonstoichiometry of ZrO_2 ($\delta=2$ for the ZrO_2/Zr bulk couple vs. $\delta=0.0625$ for the $Zr_{16}O_{32}/Zr_{16}O_{31}$ surface model couple), $Y_2Zr_6O_{15}$ ($\delta=2$ for the ZrO_2/Zr bulk couple vs. $\delta=0.0625$ for the $Y_4Zr_{12}O_{30}/Y_4Zr_{12}O_{29}$ surface model couple), CeO_2 ($\delta=1$ for the CeO_2/Ce_2O_3 bulk couple vs. $\delta=0.0625$ for the $Ce_{16}O_{32}/Ce_{16}O_{31}$ surface model couple), and of factor 3, which is relatively high when compared to the other computed perovskite models, for $La_{0.67}Sr_{0.33}MnO_3$ ($\delta=1$ for the Mn_2O_3/MnO bulk couple vs. $\delta=0.33$ for the $La_2SrMn_3O_9/La_2SrMn_3O_8$ surface model couple).

Calculations of $\Delta\bar{g}_{O_2}^o$ at 1200 K to 1800 K and $-\Delta\bar{g}_{O_2}^o$ at 800 K to 1400 K for metal oxides where the underpinning thermochemical data is not available, namely the perovskites evaluated in this work, were based on the scaling of these two bulk quantities with $\Delta\bar{h}_{O_2}^o$ at 298 K and 1 bar across 27 solid metal oxide and six metal/metal oxide pairs. Thermodynamic properties obtained through scaling relations are defined per mole of monoatomic oxygen. The data for the derived linear scaling relations ($R^2 > 0.83$) are shown with Table S2 and Table S3, where a and b represent the following factors in Eq. (4):

$$-\Delta\bar{g}_{O_2}^o = a \cdot \frac{\text{kJ mol}_{O_2}^{-1}}{\text{kJ mol}_{O_2}^{-1}} \Delta\bar{h}_{O_2}^o + b \text{ kJ mol}_{O_2}^{-1} \quad (4)$$

Table S2. DFT-derived linear scaling factors a and b, based on the scaling of $-\Delta\bar{g}_{O_2}^o$ with a stoichiometric amount of CO_2 in the inlet gas and $\Delta\bar{h}_{O_2}^o$ at 298 K and 1 bar across 27 solid metal oxide and six metal/metal oxide pairs.

T (K)	a	b
800	-0.9622	552.73
900	-0.9633	555.07
1000	-0.9647	557.63
1100	-0.9654	559.59
1200	-0.9652	561.04
1300	-0.9625	561.90
1400	-0.9594	562.50

Table S3. DFT-derived linear scaling factors a and b, based on the scaling of $-\Delta\bar{g}_{O_2}^o$ with 1% CO in CO_2 in the inlet gas and $\Delta\bar{h}_{O_2}^o$ at 298 K and 1 bar across 27 solid metal oxide and six metal/metal oxide pairs.

T (K)	a	b
800	-0.9622	583.36
900	-0.9633	589.53
1000	-0.9647	595.91
1100	-0.9654	601.71
1200	-0.9652	606.99
1300	-0.9625	611.67
1400	-0.9594	616.10

Table S4. DFT-derived linear scaling factors a and b, based on the scaling of $\Delta\bar{g}_{O_2}^o$ at $pO_2 = 10^{-4}$ bar with $\Delta\bar{h}_{O_2}^o$ at 298 K and 1 bar across 27 solid metal oxide and six metal/metal oxide pairs.

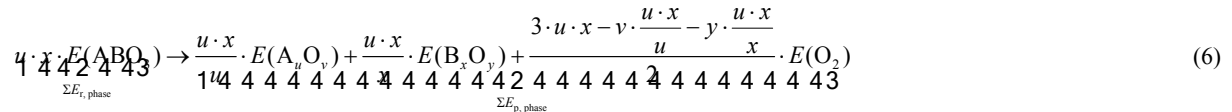
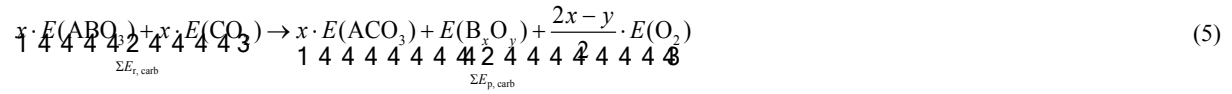
T (K)	a	b
1200	0.9652	-296.51
1300	0.9625	-322.25
1400	0.9594	-347.67
1500	0.9551	-372.30
1600	0.9514	-396.93
1700	0.9452	-419.97

| 1800 | 0.9337 | -435.95 |

The data for the derived linear scaling relations is given with Tables S5-S8. The free energies of the oxide oxidation and reduction of the computed perovskites are not shown here, but can be provided on demand.

d. Stability computations

Eq. 5 displays the schematic reaction between an ABO_3 perovskite and CO_2 , forming a carbonate and a metal oxide with the B cation. Eq. 6 illustrates the dissociation of an ABO_3 perovskite into A and B metal oxides.



where $E(\text{ABO}_3)$, $E(\text{CO}_2)$, $E(\text{ACO}_3)$, $E(\text{O}_2)$, $E(\text{A}_u\text{O}_v)$ and $E(\text{B}_x\text{O}_y)$ are the DFT total energies of the ABO_3 , CO_2 , ACO_3 , O_2 , A_uO_v and B_xO_y compound, respectively. $E(\text{O}_2)$ was taken as the energy reference of stable H_2O and H_2 in the gas phase, due to the difficulty of DFT to describe the triplet state of O_2 correctly⁹.

2. Supporting data

a. Experimental data

i. XRD of CeCoO_3

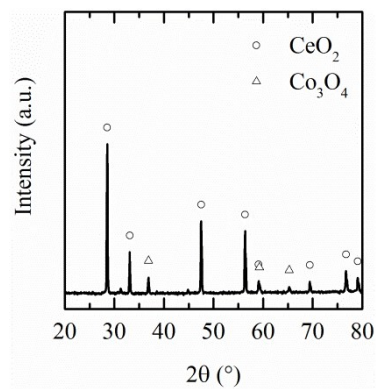


Figure S1: XRD spectrum of as-prepared CeCoO_3 (peak labels from Wolcyrz *et al.*¹⁰ and Smith *et al.*¹¹).

ii. XRD of as-prepared perovskites to be tested via TGA

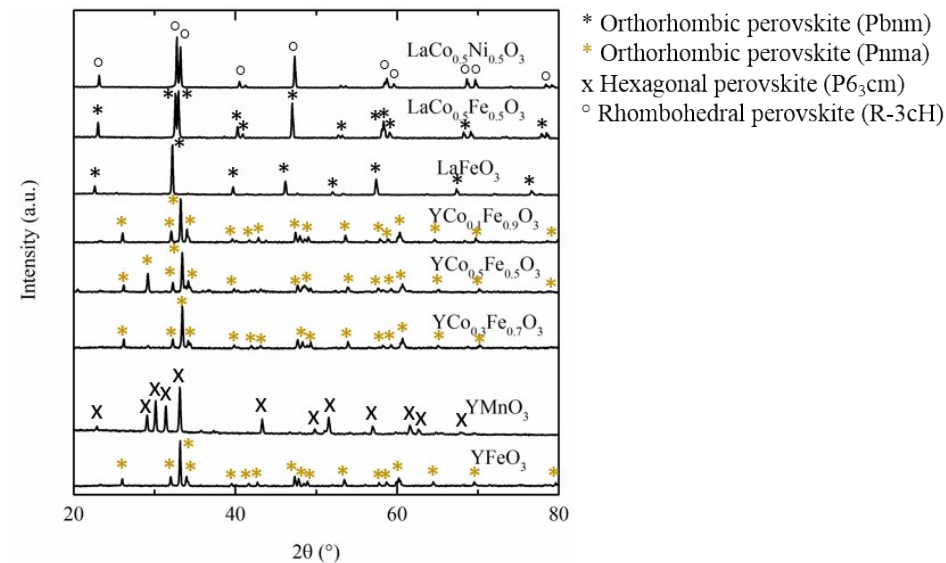


Figure S2: RT-XRDs of as-prepared YFeO_3 , YMnO_3 , $\text{YCo}_{0.3}\text{Fe}_{0.7}\text{O}_3$, $\text{YCo}_{0.5}\text{Fe}_{0.5}\text{O}_3$, $\text{YCo}_{0.1}\text{Fe}_{0.9}\text{O}_3$, LaFeO_3 , $\text{LaCo}_{0.5}\text{Fe}_{0.5}\text{O}_3$ and $\text{LaCo}_{0.5}\text{Ni}_{0.5}\text{O}_3$. Peak labels for YFeO_3 , $\text{YCo}_{0.3}\text{Fe}_{0.7}\text{O}_3$, $\text{YCo}_{0.5}\text{Fe}_{0.5}\text{O}_3$ and $\text{YCo}_{0.1}\text{Fe}_{0.9}\text{O}_3$ from du Boulay *et al.*¹², for YMnO_3 from Gibbs *et al.*¹³, for LaFeO_3 from Marezio *et al.*¹⁴, for $\text{LaCo}_{0.5}\text{Fe}_{0.5}\text{O}_3$ from McCready *et al.*¹⁵ and for $\text{LaCo}_{0.5}\text{Ni}_{0.5}\text{O}_3$ from Vyshatko *et al.*¹⁶.

iii. Oxygen nonstoichiometry

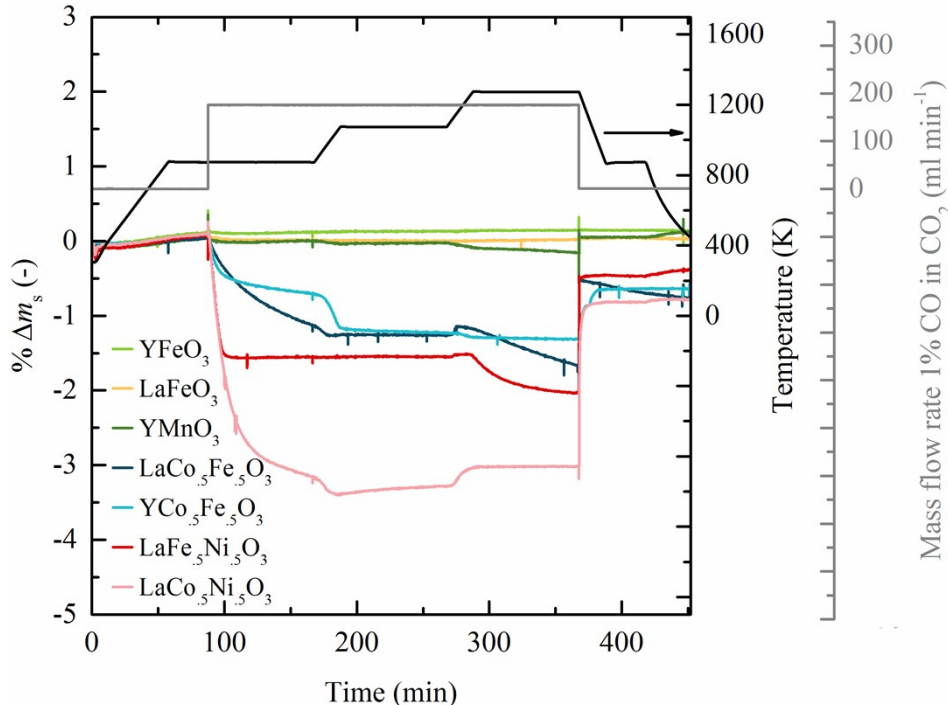


Figure S3: Percent mass change as a function of time subjected to 873, 1073 and 1273 K in 1% CO in CO_2 ($p\text{O}_2 = 1.88 \cdot 10^{-21}$, $3.79 \cdot 10^{-15}$ and $7.75 \cdot 10^{-11}$ bar O_2 , respectively) for oxidation experiments of $\text{LaCo}_{0.5}\text{Fe}_{0.5}\text{O}_3$, $\text{LaFe}_{0.5}\text{Ni}_{0.5}\text{O}_3$, $\text{LaCo}_{0.5}\text{Ni}_{0.5}\text{O}_3$, LaFeO_3 , YMnO_3 , YFeO_3 and $\text{YCo}_{0.5}\text{Fe}_{0.5}\text{O}_3$.

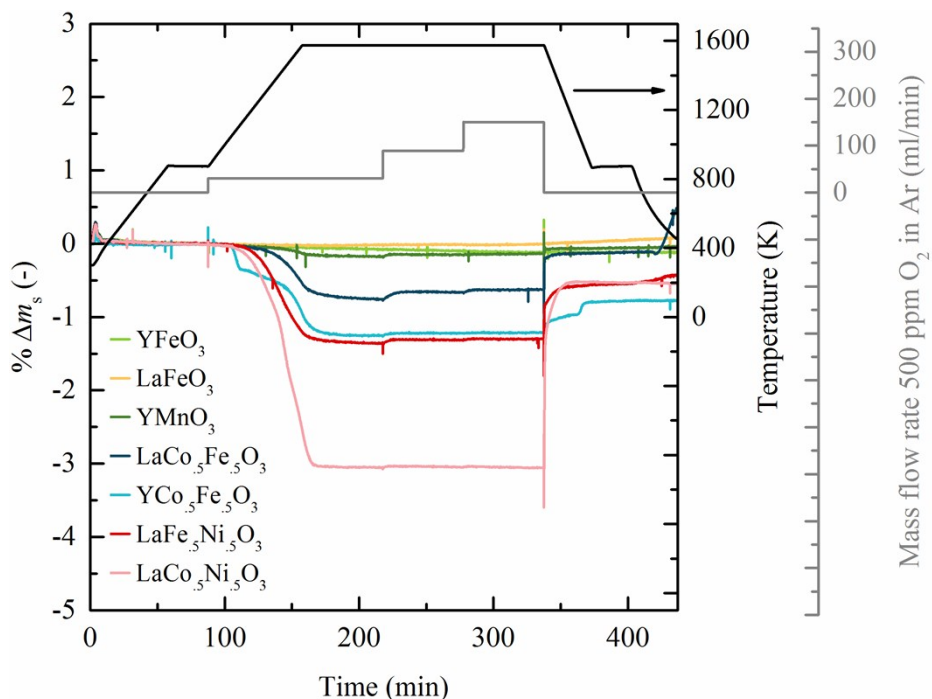


Figure S4: Percent mass change as a function of time subjected to $1 \cdot 10^{-4}$, $3.04 \cdot 10^{-4}$ and $5.07 \cdot 10^{-4}$ bar O_2 for reduction experiments of $\text{LaCo}_{0.5}\text{Fe}_{0.5}\text{O}_3$, $\text{LaFe}_{0.5}\text{Ni}_{0.5}\text{O}_3$, $\text{LaCo}_{0.5}\text{Ni}_{0.5}\text{O}_3$, LaFeO_3 , YMnO_3 , YFeO_3 and $\text{YCo}_{0.5}\text{Fe}_{0.5}\text{O}_3$.

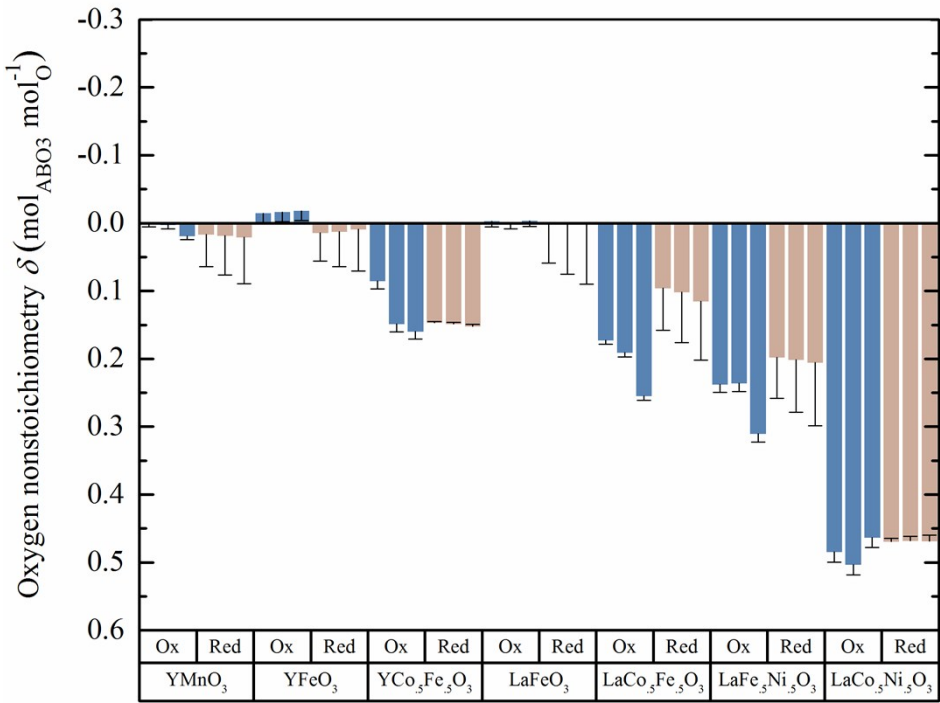


Figure S5: δ_{red} and δ_{ox} for $\text{YCo}_{0.5}\text{Fe}_{0.5}\text{O}_3$, $\text{LaFe}_{0.5}\text{Ni}_{0.5}\text{O}_3$, $\text{LaCo}_{0.5}\text{Ni}_{0.5}\text{O}_3$, YMnO_3 , LaFeO_3 , YFeO_3 and $\text{LaCo}_{0.5}\text{Fe}_{0.5}\text{O}_3$. δ_{red} results from reduction at 1573 K and $5.07 \cdot 10^{-4}$, $3.04 \cdot 10^{-4}$ and $1 \cdot 10^{-4}$ bar O_2 (beige bars, from left to right). δ_{ox} results from oxidation at 873, 1073 and 1273 K and 1% CO in CO_2 ($p\text{O}_2 = 1.88 \cdot 10^{-21}$, $3.79 \cdot 10^{-15}$ and $7.75 \cdot 10^{-11}$ bar O_2 , respectively, blue bars).

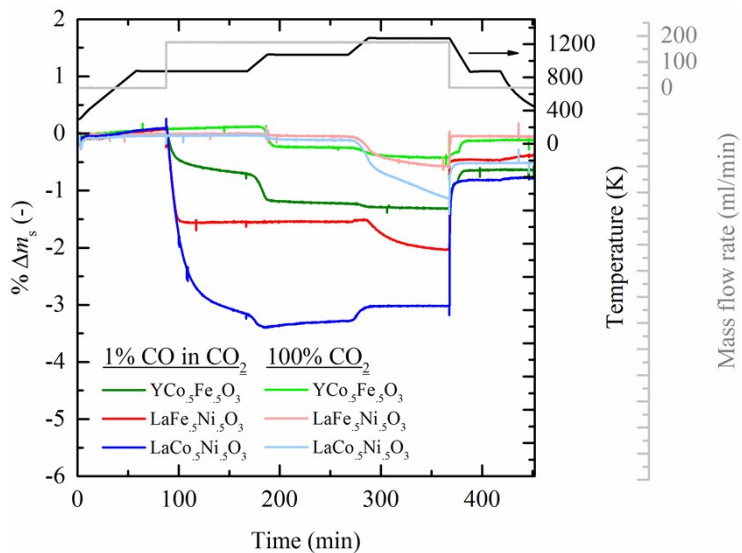


Figure S6: Percent mass change as a function of time at 873, 1073 and 1273 K in 1% CO in CO_2 ($p\text{O}_2 = 1.88 \cdot 10^{-21}$, $3.79 \cdot 10^{-15}$ and $7.75 \cdot 10^{-11}$ bar O_2 , respectively) and 100% CO_2 ($p\text{O}_2 = 3.67 \cdot 10^{-9}$, $4.63 \cdot 10^{-7}$ and $1.27 \cdot 10^{-5}$ bar O_2 , respectively) for oxidation experiments of $\text{LaFe}_{0.5}\text{Ni}_{0.5}\text{O}_3$, $\text{LaCo}_{0.5}\text{Ni}_{0.5}\text{O}_3$ and $\text{YCo}_{0.5}\text{Fe}_{0.5}\text{O}_3$.

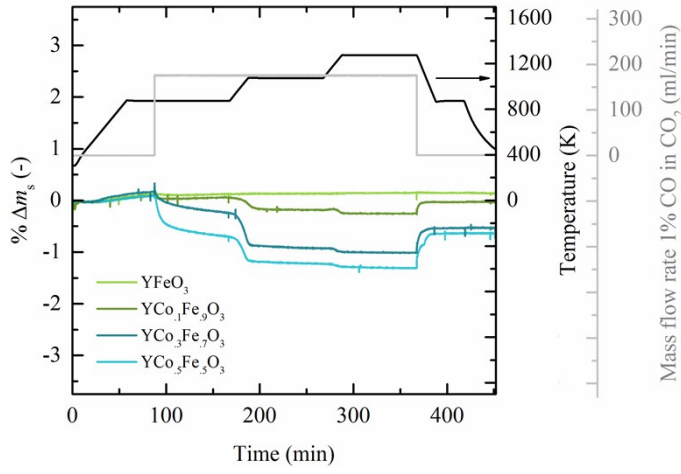


Figure S7: Percent mass change as a function of time at 873, 1073 and 1273 K in 1% CO in CO₂ ($p_{O_2} = 1.88 \cdot 10^{-21}$, $3.79 \cdot 10^{-15}$ and $7.75 \cdot 10^{-11}$ bar O₂, respectively) for oxidation experiments of YFeO₃, YCo_{0.1}Fe_{0.9}O₃ YCo_{0.3}Fe_{0.7}O₃ and YCo_{0.5}Fe_{0.5}O₃.

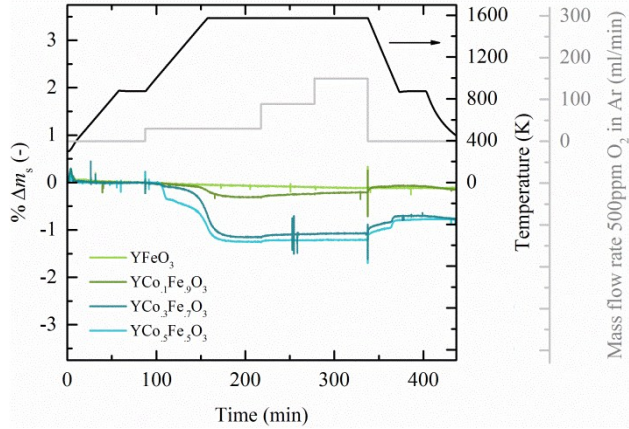


Figure S8: Percent mass change as a function of time at 1573 K in $1 \cdot 10^{-4}$, $3.04 \cdot 10^{-4}$ and $5.07 \cdot 10^{-4}$ bar O₂ for reduction experiments of YFeO₃, YCo_{0.1}Fe_{0.9}O₃ YCo_{0.3}Fe_{0.7}O₃ and YCo_{0.5}Fe_{0.5}O₃.

iv. TGA

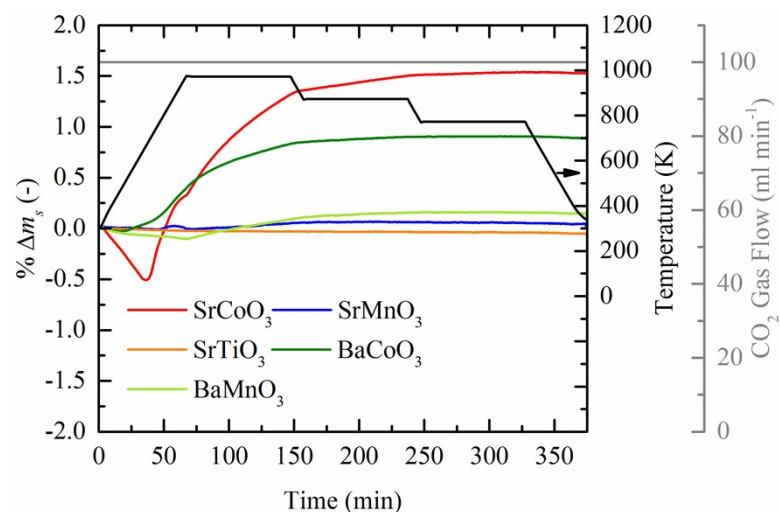


Figure S9: Percent mass change as a function of time for BaCoO₃, SrCoO₃, BaMnO₃, SrMnO₃ and SrTiO₃.

v. HT-XRD for material stability

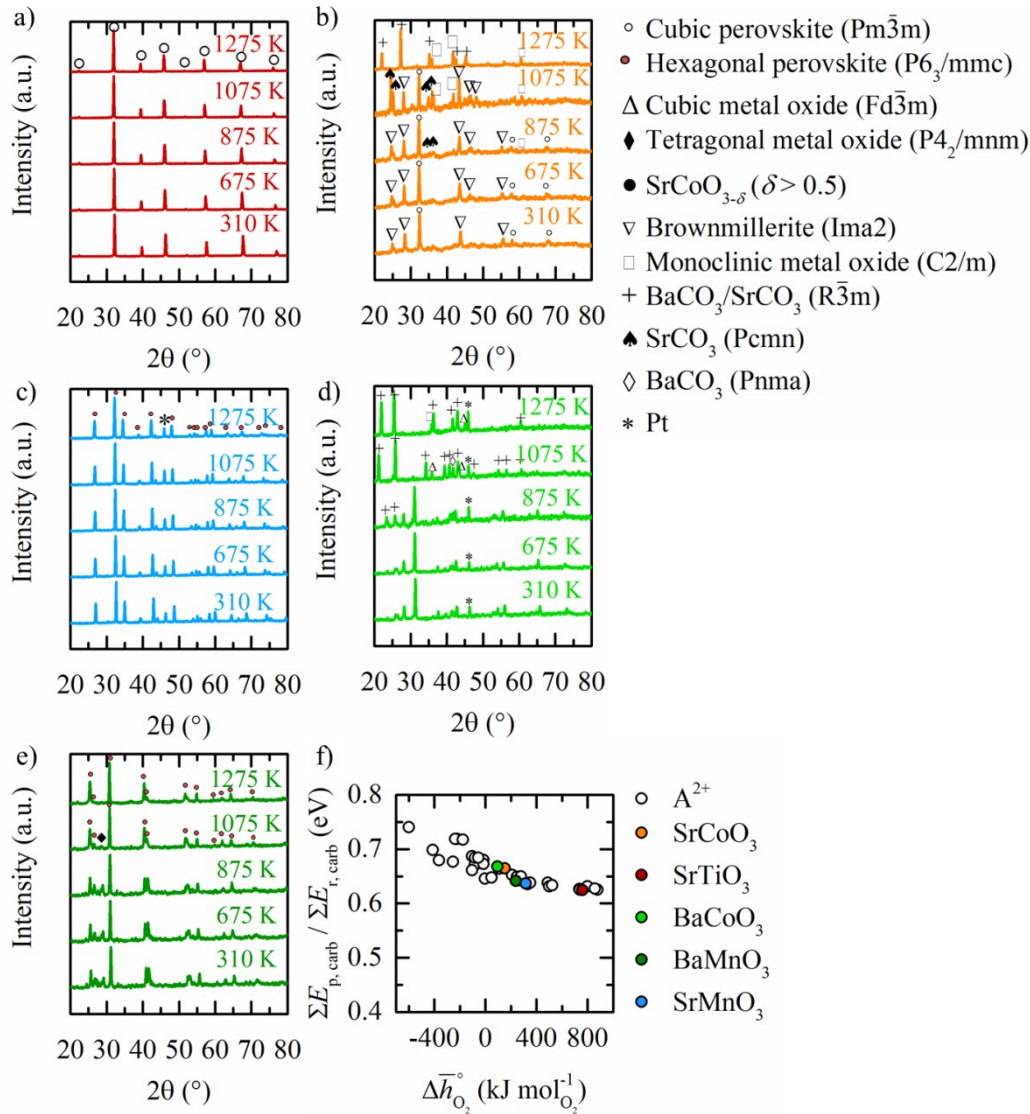


Figure S10: HT-XRD spectra in CO_2 between 310 and 1275 K of a) SrTiO_3 (peak labels from Howard *et al.*¹⁷) and b) SrCoO_3 (peak labels from Wang *et al.*¹⁸, Zeng *et al.*¹⁹, Saito *et al.*²⁰, Hanawalt *et al.*²¹ and Stromme *et al.*²²), c) SrMnO_3 (peak labels from Kuroda *et al.*²³), d) BaCoO_3 (peak labels from Jacobson *et al.*²⁴, Liu *et al.*²⁵, Stromme *et al.*²², Bell *et al.*²⁶ and Saito *et al.*²⁰) and e) BaMnO_3 (peak labels from Negas *et al.*²⁷, Liu *et al.*²⁸ and McMurdie *et al.*²⁹) and f) ratio between $\sum E_{\text{p, carb}}$ and $\sum E_{\text{r, carb}}$ for 36 ABO_3 -type perovskites with divalent A-cations (round symbols), with SrTiO_3 , SrCoO_3 , SrMnO_3 , BaCoO_3 and BaMnO_3 highlighted in orange, red, light green, dark green and light blue, respectively.

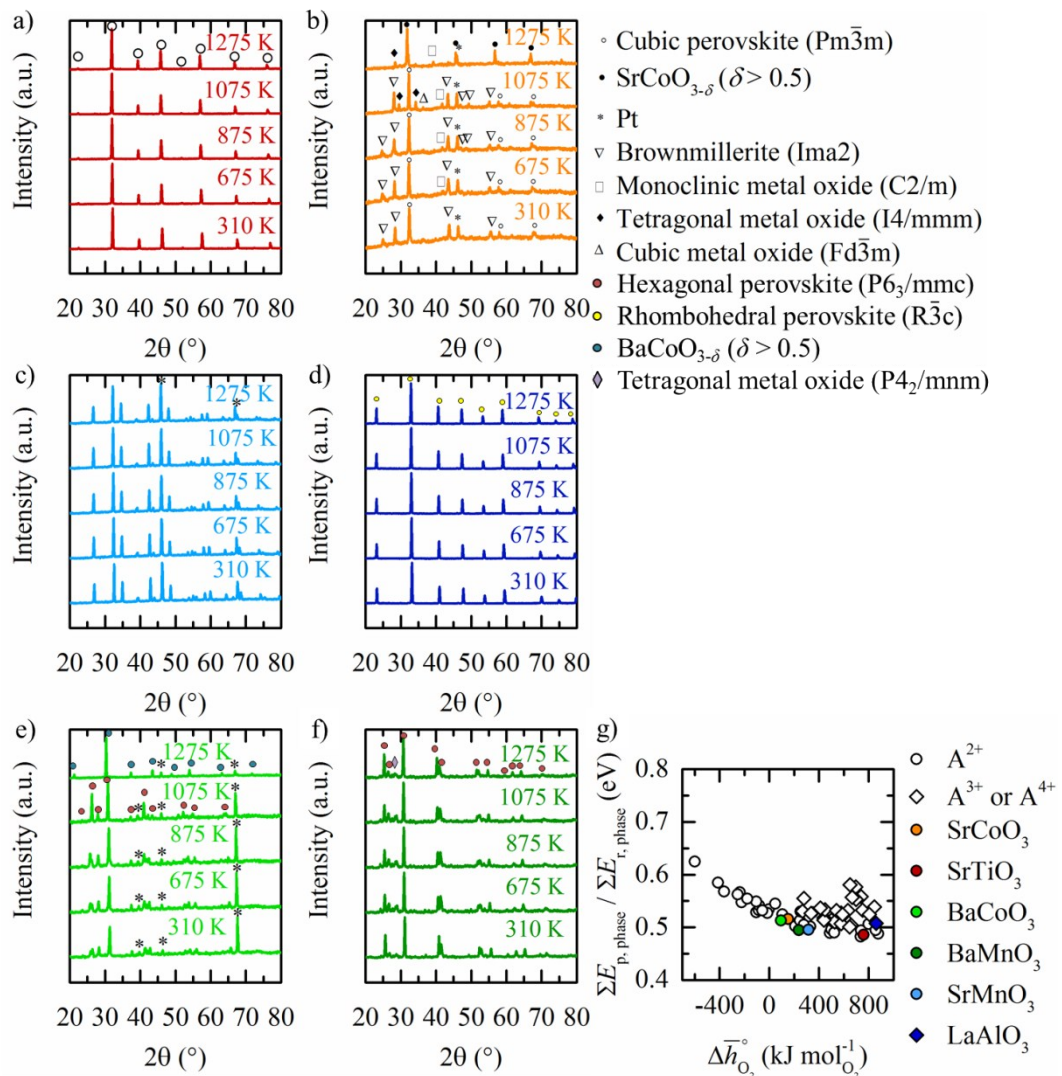


Figure S11: HT-XRD spectra in 0.2 bar O_2 between 310 and 1275 K of a) SrTiO_3 (peak labels from Howard *et al.*¹⁷) and b) SrCoO_3 (peak labels from Wang *et al.*¹⁸, Zeng *et al.*¹⁹, Davey *et al.*³⁰, Hanawalt *et al.*²¹, Saito *et al.*²⁰, Takeda *et al.*³¹ and Liu *et al.*²⁵), c) SrMnO_3 (peak labels from Kuroda *et al.*²³), d) LaAlO_3 (peak labels from Lehnert *et al.*³²), e) BaCoO_3 (peak labels from Jacobson *et al.*²⁴ and Spitsbergen *et al.*³³), f) BaMnO_3 (peak labels from Negas *et al.*²⁷ and McMurdie *et al.*²⁹) and g) ratio between $\sum E_{\text{p, phase}}$ and $\sum E_{\text{r, phase}}$ for 63 ABO_3 -type perovskites with divalent A-cations (round symbols) and trivalent and tetravalent A-cations (square symbols), with SrCoO_3 , SrTiO_3 , SrMnO_3 , BaCoO_3 , BaMnO_3 and LaAlO_3 highlighted in orange, red, light blue, light green, dark green and dark blue, respectively.

vi. RT-XRD

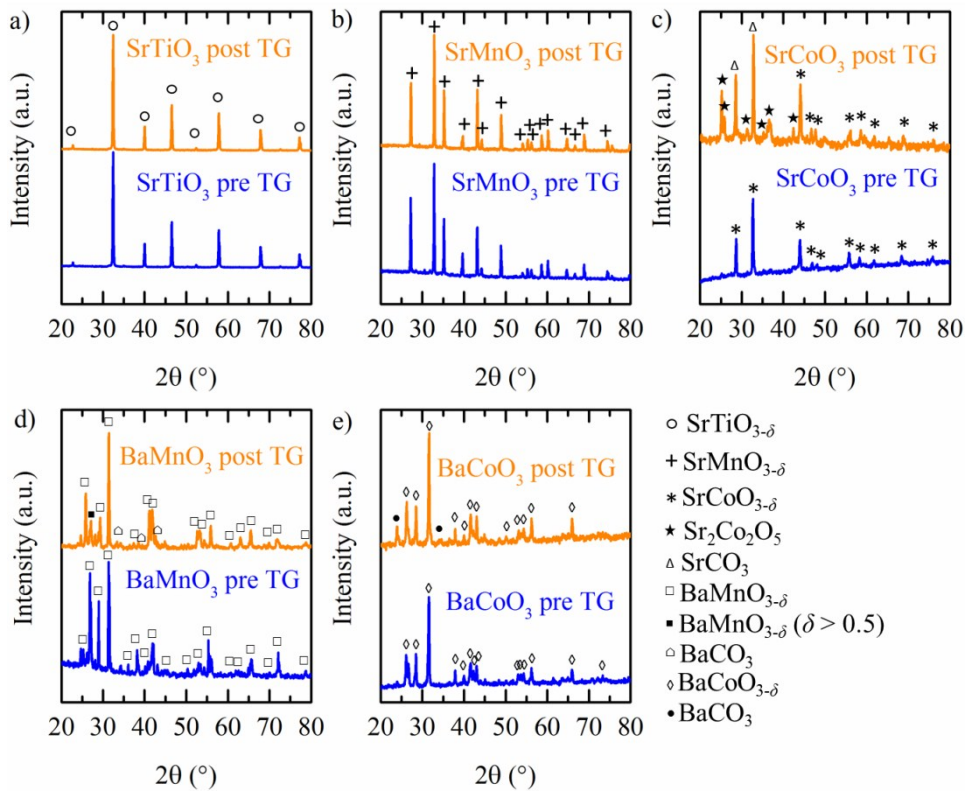


Figure S12: RT-XRD spectra before and after TGA with CO_2 of a) SrTiO_3 (peak labels from Howard *et al.*¹²), b) SrMnO_3 (peak labels from Kuroda *et al.*²³), c) SrCoO_3 (peak labels from Takeda *et al.*³¹, Grenier *et al.*³⁴ and Stromme *et al.*²²), d) BaMnO_3 (peak labels from Negas *et al.*²⁷ and Bell *et al.*²⁶) and e) BaCoO_3 (peak labels from Jacobson *et al.*²⁴ and Hanawalt *et al.*²¹).

vii. TEM

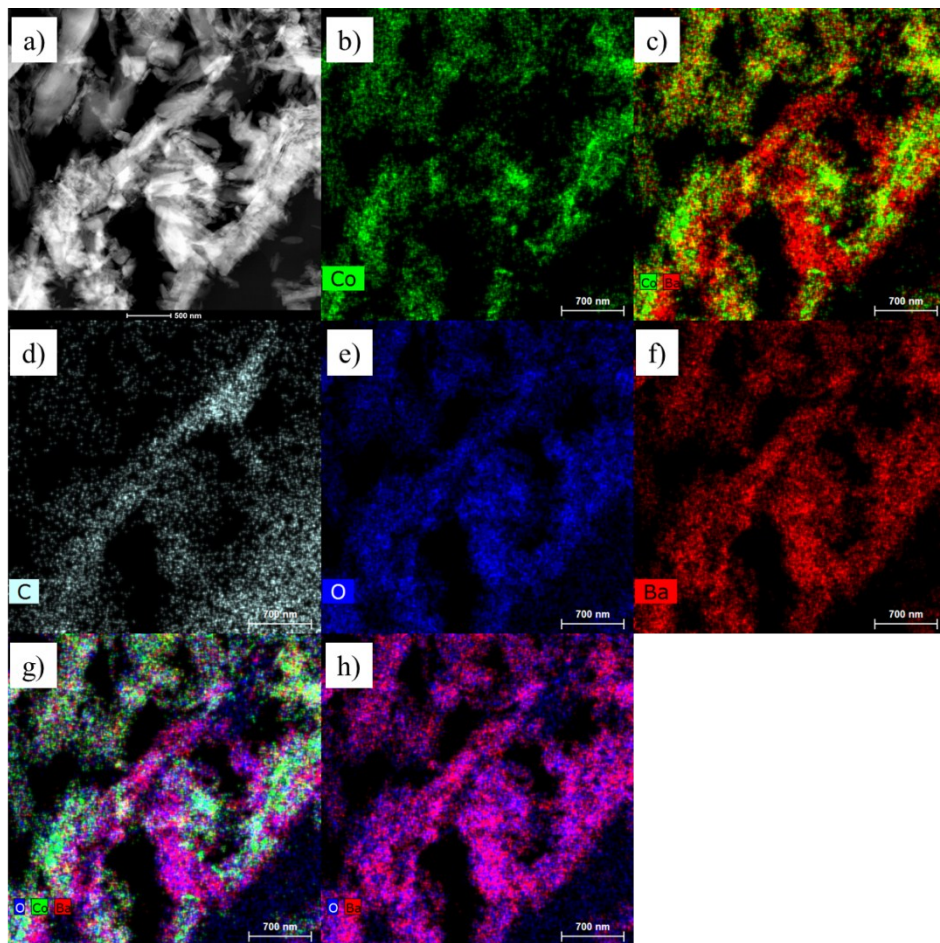


Figure S13: HAADF STEM images of BaCoO_3 : a) material flakes (bright areas) suspended over the vacuum window in the amorphous carbon support foil (the dark grey left part of the micrograph), and b-h) the drift corrected, elemental maps and their overlays.

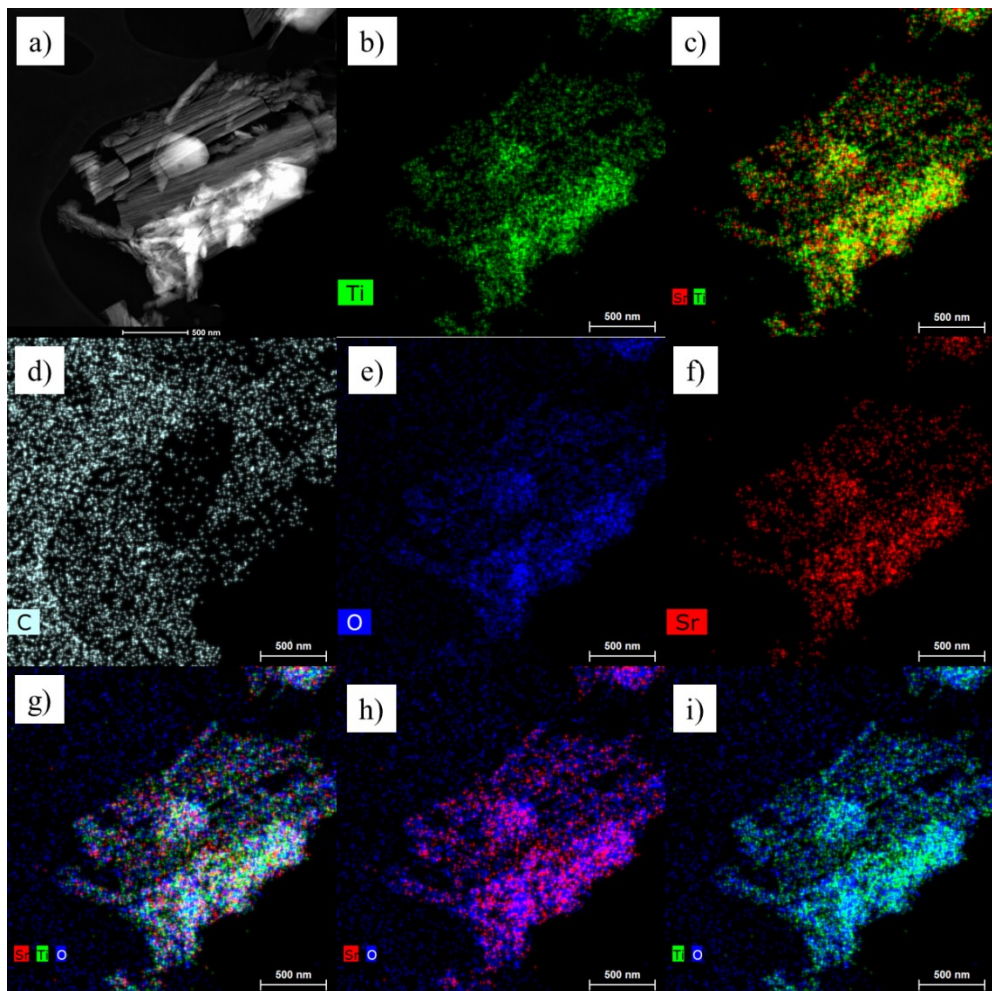


Figure S14: HAADF STEM images of SrTiO_3 : a) material flakes (bright areas) suspended over the vacuum window in the amorphous carbon support foil (the dark grey left part of the micrograph), and b-i) the drift corrected, elemental maps and their overlays.

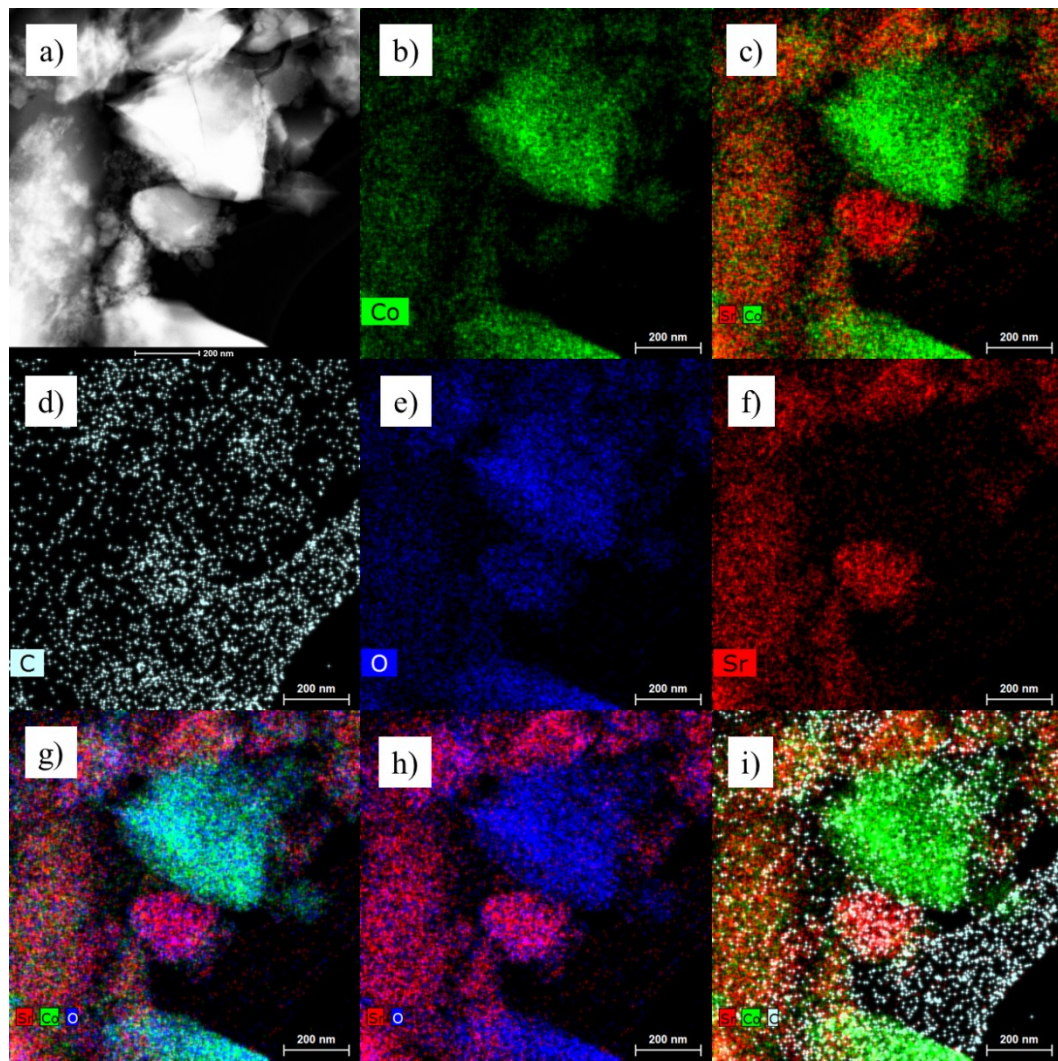


Figure S15: HAADF STEM images of SrCoO_3 : a) material flakes (bright areas) suspended over the vacuum window in the amorphous carbon support foil (the dark grey left part of the micrograph), and b-i) the drift corrected, elemental maps and their overlays.

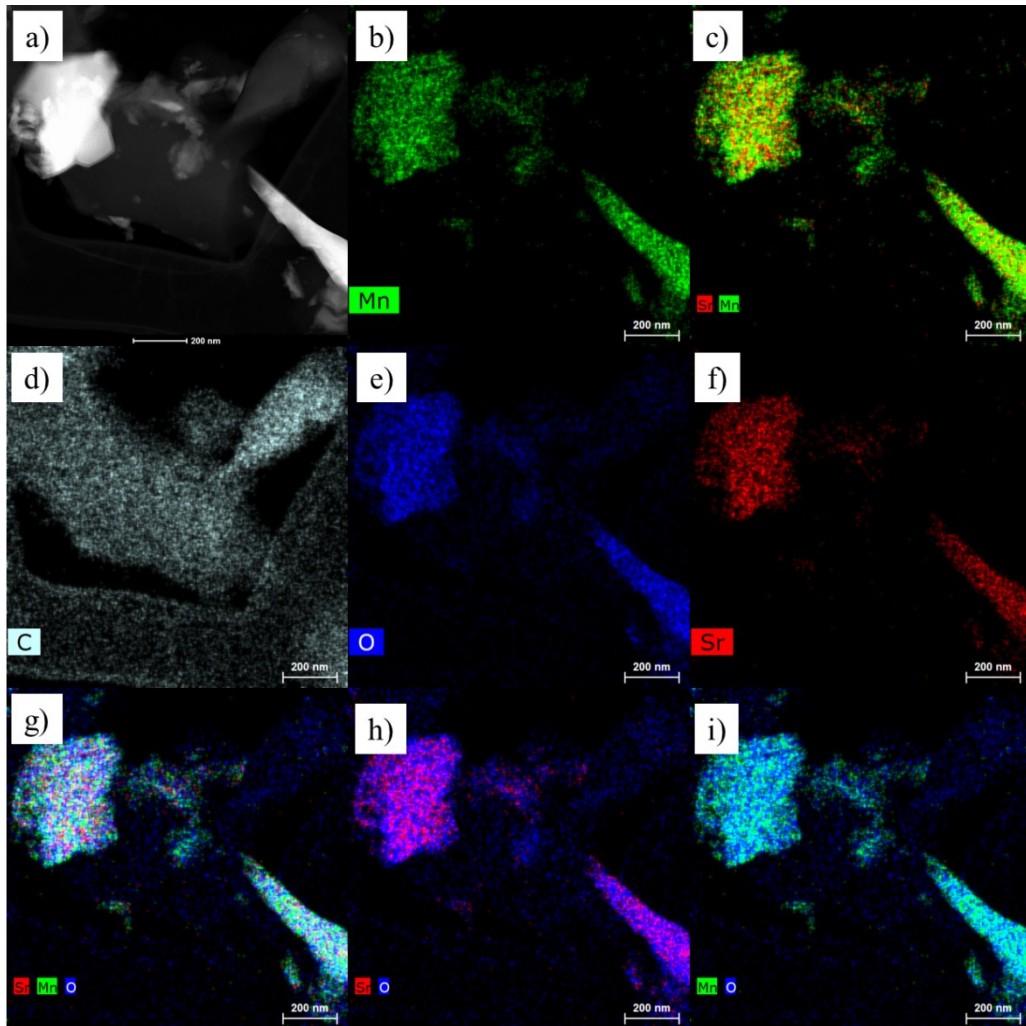


Figure S16: HAADF STEM images of SrMnO_3 : a) material flakes (bright areas) suspended over the vacuum window in the amorphous carbon support foil (the dark grey left part of the micrograph), and b-f) the drift corrected, elemental maps and their overlays.

b. Thermochemical equilibrium analysis

Thermochemical data³⁵ was extrapolated for $\text{Ce}_2\text{O}_3 \geq 1300 \text{ K}$, $\text{Co}_3\text{O}_4 \geq 1300 \text{ K}$, $\text{CuO} \geq 1400 \text{ K}$, $\text{Fe}_2\text{O}_3 \geq 1800 \text{ K}$, $\text{Mn}_3\text{O}_4 \geq 1900 \text{ K}$, $\text{Mn}_2\text{O}_3 \geq 1500 \text{ K}$, $\text{MoO}_3 \geq 1500 \text{ K}$, $\text{Na}_2\text{O}_2 \geq 1000 \text{ K}$, $\text{RhO} \geq 1200 \text{ K}$, $\text{Rh}_2\text{O}_3 \geq 1400 \text{ K}$, $\text{RuO}_2 \geq 1400 \text{ K}$, $\text{Sb}_2\text{O}_3 \geq 1800 \text{ K}$, $\text{SbO}_2 \geq 1300 \text{ K}$, $\text{SnO} \geq 1400 \text{ K}$, $\text{SnO}_2 \geq 1600 \text{ K}$, $\text{Tl}_2\text{O} \geq 1100 \text{ K}$, and $\text{Tl}_2\text{O}_3 \geq 1200 \text{ K}$ using second-order polynomial regressions with R^2 between 0.99932 and 0.99998.

Table S5. Enthalpies of reduction at 298 K ($\Delta\bar{h}_{\text{O}_2}^\circ$) and Gibbs free energies of the oxide reduction at 298 K ($\Delta\bar{g}_{\text{O}_2}^\circ$) and oxide oxidation at 298 K ($-\Delta\bar{g}_{\text{O}_2}^\circ$) of 27 solid metal oxide and six metal/metal oxide pairs at 1 bar, calculated from experiment-derived tabulated thermochemical data.³⁵

Product of the oxide oxidation	Reactant of the oxide oxidation	$\Delta\bar{h}_{\text{O}_2}^\circ$ (kJ mol $_{\text{O}_2}^{-1}$)	$\Delta\bar{g}_{\text{O}_2}^\circ$ (kJ mol $_{\text{O}_2}^{-1}$)	$-\Delta\bar{g}_{\text{O}_2}^\circ$ (kJ mol $_{\text{O}_2}^{-1}$)
Ag_2O	Ag	62.20	21.63	492.74
Au_2O_3	Au	-53.84	-51.86	566.22
CeO_2	Ce_2O_3	762.33	685.67	-171.30
Co_3O_4	CoO	392.38	304.62	209.75

Cu ₂ O	Cu	237.77	217.06	297.31
CuO	Cu ₂ O	351.62	295.25	219.12
Fe _{0.947} O	FeO	604.50	521.81	-7.44
Fe ₂ O ₃	Fe ₃ O ₄	471.96	392.85	121.52
Fe ₃ O ₄	FeO	464.27	389.07	125.29
Mn ₃ O ₄	MnO	202.82	153.75	360.61
Mn ₂ O ₃	Mn ₃ O ₄	312.29	269.89	244.48
MoO ₃	MoO ₂	190.45	141.08	373.29
Na ₂ O ₂	Na ₂ O	750.61	694.51	-180.14
NbO ₂	NbO	619.23	574.94	-60.57
Nb ₂ O ₅	NbO ₂	345.02	331.81	182.55
Rh ₂ O ₃	RhO	305.01	253.02	261.35
RuO ₂	Ru	338.09	319.70	194.67
SbO ₂	Sb ₂ O ₃	590.11	526.30	-11.93
SnO ₂	SnO	871.11	814.54	-300.17
Ti ₂ O ₃	TiO	711.28	666.23	-151.86
Ti ₃ O ₅	Ti ₂ O ₃	753.96	739.75	-225.38
Ti ₄ O ₇	Ti ₃ O ₅	748.93	689.21	-174.85
TiO ₂	Ti ₄ O ₇	185.40	162.72	351.65
Tl ₂ O ₃	Tl ₂ O	710.44	661.25	-146.89
V ₂ O ₃	VO	416.73	358.81	155.56
V ₂ O ₄	V ₂ O ₃	246.86	201.81	312.56
V ₂ O ₅	V ₂ O ₄	531.83	485.47	28.90
WO _{2.72}	WO ₂	432.34	387.67	126.70
WO _{2.9}	WO _{2.72}	496.50	450.34	64.03
WO _{2.96}	WO _{2.9}	397.50	351.29	163.08
WO ₃	WO _{2.96}	341.41	295.35	219.01
ZnO	Zn	700.92	640.95	-126.59
ZrO ₂	Zr	1097.46	1039.72	-525.36

Table S6. Gibbs free energies of the oxide oxidation between 800 K and 1400 K ($-\Delta\bar{g}_{O_2}^{\circ}$) of 27 solid metal oxide and six metal/metal oxide pairs in 100% CO₂, calculated from experiment-derived tabulated thermochemical data.³⁵

Product of oxide oxidation	Reactant of oxide oxidation	$-\Delta\bar{g}_{O_2}^{\circ}$ (kJ mol _{O₂} ⁻¹)						
		800 K	900 K	1000 K	1100 K	1200 K	1300 K	1400 K
Ag ₂ O	Ag	490.92	497.25	505.33	515.03	526.23	541.29	558.97
Au ₂ O ₃	Au	577.56	583.08	589.47	596.67	604.61	613.27	623.40
CeO ₂	Ce ₂ O ₃	-125.80	-115.85	-105.63	-95.13	-84.38	-67.34	-50.44
Co ₃ O ₄	CoO	287.61	304.33	320.80	336.84	352.336	362.51	372.32
CuO	Cu ₂ O	313.71	315.71	317.43	318.88	320.09	321.09	317.25
Cu ₂ O	Cu	219.73	219.26	218.81	218.43	218.086	217.79	217.55
Fe _{0.947} O	FeO	38.34	43.88	48.67	53.27	57.90	62.69	67.67
Fe ₂ O ₃	Fe ₃ O ₄	171.16	183.63	195.69	207.27	218.82	230.22	241.41
Fe ₃ O ₄	FeO	164.25	171.68	178.94	186.01	192.88	199.51	205.91
Mn ₃ O ₄	MnO	353.08	351.20	349.24	347.21	345.09	342.90	340.62
Mn ₂ O ₃	Mn ₃ O ₄	224.972	220.67	216.29	209.54	195.68	181.52	167.12
MoO ₃	MoO ₂	364.20	360.41	354.82	348.06	339.60	330.28	319.71
Na ₂ O ₂	Na ₂ O	-176.95	-177.13	-177.58	-178.40	-180.10	-182.01	-184.02
NbO ₂	NbO	-75.57	-78.40	-80.91	-82.88	-83.22	-83.24	-83.12
Nb ₂ O ₅	NbO ₂	216.17	223.26	230.46	237.71	248.63	259.70	267.07
Rh ₂ O ₃	RhO	256.95	255.48	253.91	252.25	250.52	248.72	245.13
RuO ₂	Ru	221.49	228.92	245.83	266.49	287.28	303.34	319.66
SbO ₂	Sb ₂ O ₃	4.34	6.15	7.79	9.30	10.72	12.06	15.62
SnO ₂	SnO	-301.94	-303.98	-306.25	-308.65	-311.13	-313.17	-314.30
Ti ₂ O ₃	TiO	-192.09	-199.22	-205.31	-210.56	-215.16	-219.27	-223.04
Ti ₃ O ₅	Ti ₂ O ₃	-206.79	-198.92	-191.82	-185.26	-178.99	-172.79	-166.46
Ti ₄ O ₇	Ti ₃ O ₅	-160.04	-156.27	-152.17	-147.73	-142.97	-137.882	-132.49
TiO ₂	Ti ₄ O ₇	360.56	363.52	368.37	372.11	374.96	378.71	382.62
Tl ₂ O ₃	Tl ₂ O	-154.02	-155.66	-157.25	-158.75	-160.16	-161.474	-162.69

V ₂ O ₃	VO	139.27	135.20	131.064	126.90	122.73	118.57	114.44
V ₂ O ₄	V ₂ O ₃	323.25	325.54	319.96	308.32	296.58	284.78	272.96
V ₂ O ₅	V ₂ O ₄	15.88	12.86	9.79	6.67	3.51	0.31	-2.94
WO _{2.72}	WO ₂	110.74	107.08	103.37	99.63	95.89	92.15	88.42
WO _{2.9}	WO _{2.72}	50.60	47.31	43.97	40.59	37.11	33.592	30.06
WO _{2.96}	WO _{2.9}	155.47	154.34	152.97	147.88	140.72	135.042	130.66
WO ₃	WO _{2.96}	205.24	202.07	198.75	195.28	191.65	187.83	185.51
ZnO	Zn	-113.40	-109.31	-105.20	-101.09	-92.79	-69.22	-45.82
ZrO ₂	Zr	-518.65	-517.72	-516.84	-515.98	-514.91	-513.76	-512.64

Table S7. Gibbs free energies of the oxide oxidation between 800 K and 1400 K ($-\Delta\bar{g}_{O_2}^0$) of 27 solid metal oxide and six metal/metal oxide pairs at 1% CO in CO₂, calculated from experiment-derived tabulated thermochemical data.³⁵

Product of the oxide oxidation	Reactant of the oxide oxidation	$-\Delta\bar{g}_{O_2}^0$ (kJ mol ⁻¹)						
		800 K	900 K	1000 K	1100 K	1200 K	1300 K	1400 K
Ag ₂ O	Ag	521.55	531.71	543.62	557.15	572.17	591.07	612.58
Au ₂ O ₃	Au	608.19	617.54	627.76	638.79	650.56	663.05	677.00
CeO ₂	Ce ₂ O ₃	-95.17	-81.39	-67.34	-53.01	-38.44	-17.57	3.17
Co ₃ O ₄	CoO	318.24	338.79	359.09	378.96	398.28	412.28	425.92
CuO	Cu ₂ O	344.34	350.17	355.72	361.00	366.04	370.86	370.86
Cu ₂ O	Cu	250.36	253.72	257.10	260.55	264.03	267.57	271.16
Fe _{0.947} O	FeO	68.97	78.34	86.96	95.39	103.85	112.46	121.28
Fe ₂ O ₃	Fe ₃ O ₄	201.79	218.09	233.98	249.39	264.77	280.00	295.02
Fe ₃ O ₄	FeO	194.89	206.14	217.23	228.13	238.83	249.29	259.51
Mn ₃ O ₄	MnO	383.719	385.66	387.53	389.33	391.04	392.68	394.22
Mn ₂ O ₃	Mn ₃ O ₄	255.60	255.13	254.58	251.66	241.63	231.30	220.72
MoO ₃	MoO ₂	394.83	394.87	393.11	390.18	385.54	380.05	373.32
Na ₂ O ₂	Na ₂ O	-146.32	-142.67	-139.29	-136.28	-134.15	-132.24	-130.42

NbO ₂	NbO	-44.94	-43.94	-42.62	-40.76	-37.27	-33.46	-29.52	
Nb ₂ O ₅	NbO ₂	246.80	257.72	268.75	279.83	294.58	309.47	320.68	
Rh ₂ O ₃	RhO	287.58	289.94	292.19	294.37	296.47	298.50	298.73	
RuO ₂	Ru	252.12	263.38	284.12	308.61	333.23	353.12	373.26	
SbO ₂	Sb ₂ O ₃	34.97	40.61	46.08	51.42	56.66	61.83	69.22	
SnO ₂	SnO	-271.30	-269.52	-267.96	-266.53	-265.18	-263.39	-260.69	
Ti ₂ O ₃	TiO	-161.46	-164.76	-167.02	-168.45	-169.21	-169.49	-169.43	
Ti ₃ O ₅	Ti ₂ O ₃	-176.16	-164.46	-153.53	-143.14	-133.04	-123.02	-112.86	
Ti ₄ O ₇	Ti ₃ O ₅	-129.41	-121.81	-113.88	-105.61	-97.02	-88.11	-78.89	
TiO ₂	Ti ₄ O ₇	391.19	397.98	406.66	414.23	420.91	428.49	436.22	
Tl ₂ O ₃	Tl ₂ O	-123.39	-121.20	-118.96	-116.63	-114.21	-111.70	-109.08	
V ₂ O ₃	VO	169.90	169.66	169.35	169.02	168.68	168.35	168.04	
V ₂ O ₄	V ₂ O ₃	353.89	360.00	358.25	350.44	342.53	334.55	326.57	
V ₂ O ₅	V ₂ O ₄	46.51	47.32	48.08	48.79	49.46	50.09	50.67	
WO _{2.72}	WO ₂	141.38	141.54	141.66	141.74	141.83	141.92	142.03	
WO _{2.9}	WO _{2.72}	81.23	81.77	82.26	82.71	83.05	83.37	83.66	
WO _{2.96}	WO _{2.9}	186.10	188.80	191.26	189.99	186.67	184.82	184.26	
WO ₃	WO _{2.96}	235.87	236.53	237.04	237.40	237.60	237.61	239.11	
ZnO	Zn	-82.77	-74.85	-66.91	-58.97	-46.84	-19.44	7.78	
ZrO ₂	Zr	-488.02	-483.26	-478.55	-473.87	-468.97	-463.98	-459.03	

Table S8. Gibbs free energies of the oxide reduction between 1200 K and 1800 K ($\Delta\bar{g}_{O_2}^{\circ}$) of 27 solid metal oxide and six metal/metal oxide pairs at $pO_2 = 10^{-4}$ bar, calculated from experiment-derived tabulated thermochemical data.³⁵

Product of the oxide reduction	Reactant of the oxide reduction	$\Delta\bar{g}_{O_2}^{\circ}$ (kJ mol $_{O_2}^{-1}$)						
		1200 K	1300 K	1400 K	1500 K	1600 K	1700 K	1800 K
Ag ₂ O	Ag	-261.70	-340.09	348.92	-87.81	-55.562	46.44	206.62
Au ₂ O ₃	Au	-301.65	-373.63	306.99	-122.86	-81.44	21.85	176.96

CeO ₂	Ce ₂ O ₃	-344.15	-408.57	265.26	-157.49	-102.43	-2.73	147.15	
Co ₃ O ₄	CoO	-387.87	-444.52	221.56	-189.91	-123.79	-27.17	117.19	
CuO	Cu ₂ O	-432.71	-481.00	175.76	-220.00	-150.58	-51.54	87.07	
Cu ₂ O	Cu	-478.63	-517.95	127.77	-247.63	-176.54	-66.91	52.42	
Fe _{0.947} O	FeO	-525.54	-555.37	77.50	-272.71	-200.88	-73.38	13.17	
Fe ₂ O ₃	Fe ₃ O ₄	-261.70	-340.08	348.91	-87.81	-55.56	46.44	206.62	
Fe ₃ O ₄	FeO	-301.65	-373.63	306.99	-122.86	-81.44	21.85	176.96	
Mn ₃ O ₄	MnO	-344.15	-408.57	265.26	-157.49	-102.43	-2.73	147.15	
Mn ₂ O ₃	Mn ₃ O ₄	-387.87	-444.52	221.56	-189.91	-123.79	-27.17	117.19	
MoO ₃	MoO ₂	-432.71	-481.00	175.76	-220.00	-150.58	-51.54	87.07	
Na ₂ O ₂	Na ₂ O	-478.63	-517.95	127.77	-247.63	-176.543	-66.91	52.42	
NbO ₂	NbO	-525.54	-555.37	77.50	-272.71	-200.88	-73.38	13.17	
Nb ₂ O ₅	NbO ₂	-261.70	-340.08	348.91	-87.81	-55.56	46.44	206.62	
Rh ₂ O ₃	RhO	-301.65	-373.63	306.99	-122.86	-81.44	21.85	176.96	
RuO ₂	Ru	-344.15	-408.57	265.26	-157.49	-102.43	-2.73	147.15	
SbO ₂	Sb ₂ O ₃	-387.87	-444.52	221.56	-189.91	-123.79	-27.17	117.19	
SnO ₂	SnO	-432.71	-481.00	175.76	-220.00	-150.58	-51.54	87.07	
Ti ₂ O ₃	TiO	-478.63	-517.95	127.77	-247.63	-176.54	-66.91	52.42	
Ti ₃ O ₅	Ti ₂ O ₃	-525.54	-555.37	77.50	-272.71	-200.88	-73.38	13.17	
Ti ₄ O ₇	Ti ₃ O ₅	-261.70	-340.08	348.91	-87.81	-55.56	46.44	206.62	
TiO ₂	Ti ₄ O ₇	-301.65	-373.63	306.99	-122.86	-81.44	21.85	176.96	
Tl ₂ O ₃	Tl ₂ O	-344.15	-408.57	265.26	-157.49	-102.43	-2.73	147.15	
V ₂ O ₃	VO	-387.87	-444.52	221.56	-189.91	-123.79	-27.17	117.19	
V ₂ O ₄	V ₂ O ₃	-432.71	-481.00	175.76	-220.00	-150.58	-51.54	87.07	
V ₂ O ₅	V ₂ O ₄	-478.63	-517.95	127.77	-247.63	-176.54	-66.91	52.42	
WO _{2.72}	WO ₂	-525.54	-555.37	77.50	-272.71	-200.88	-73.38	13.17	
WO _{2.9}	WO _{2.72}	-261.70	-340.08	348.91	-87.81	-55.56	46.44	206.62	
WO _{2.96}	WO _{2.9}	-301.65	-373.63	306.99	-122.86	-81.44	21.85	176.96	
WO ₃	WO _{2.96}	-344.15	-408.57	265.26	-157.49	-102.43	-2.73	147.15	
ZnO	Zn	-387.87	-444.52	221.56	-189.91	-123.79	-27.17	117.19	
ZrO ₂	Zr	-432.71	-481.00	175.76	-220.00	-150.58	-51.54	87.07	

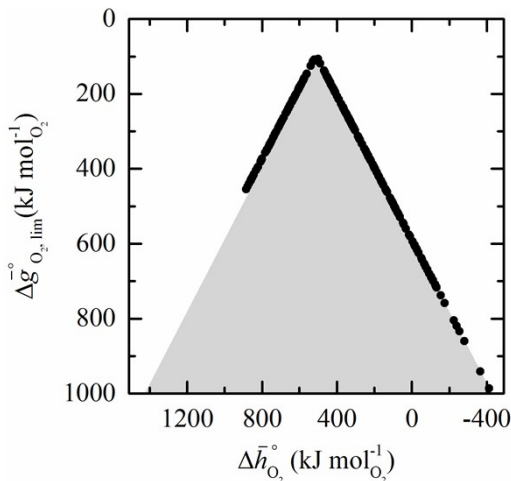


Figure S17: $\Delta g_{O_2,lim}^{\circ}$ (reduction: 10^{-4} bar O₂, 1600 K, oxidation: 1% CO in CO₂, 900 K) vs. $\Delta h_{O_2}^{\circ}$ for 297 perovskite models.

3. References

- 1 Medford, A. J.; Vojvodic, A.; Studt, F.; Abild-Pedersen, F.; Nørskov, J. K., *J. Catal.*, **2012**, *290*, 108-117.
- 2 Medford, A. J.; Wellendorff, J.; Vojvodic, A.; Studt, F.; Abild-Pedersen, F.; Jacobsen, K. W.; Bligaard, T.; Nørskov, J. K., *Science*, **2014**, *345*, 197-200.
- 3 Tsui, F.; Smoak, M. C.; Nath, T. K.; Eom, C. B., *Appl. Phys. Lett.*, **2000**, *76*, 2421-2423.
- 4 Hardy, J. S.; Templeton, J. W.; Edwards, D. J.; Lu, Z. G.; Stevenson, J. W., *J. Power Sources*, **2012**, *198*, 76-82.
- 5 Hashimoto, S.; Fukuda, Y.; Kuhn, M.; Sato, K.; Yashiro, K.; Mizusaki, J., *Solid State Ionics*, **2011**, *186*, 37-43.
- 6 Bezdicka, P.; Wattiaux, A.; Grenier, J. C.; Pouchard, M.; Hagenmuller, P., *Z. Anorg. Allg. Chem.*, **1993**, *619*, 7-12.
- 7 Zeng, Z. H.; Calle-Vallejo, F.; Mogensen, M. B.; Rossmeisl, J., *PCCP*, **2013**, *15*, 7526-7533.
- 8 Michalsky, R.; Botu, V.; Hargus, C. M.; Peterson, A. A.; Steinfeld, A., *Adv. Energy Mater.*, **2014**, *4*, 1401082.
- 9 Rossmeisl, J.; Logadottir, A.; Nørskov, J. K., *Chem. Phys.*, **2005**, *319*, 178-184.
- 10 Wolcyrz, M.; Kepinski, L., *J. Solid State Chem.*, **1992**, *99*, 409-413.
- 11 Smith, W. L.; Hobson, A. D., *Acta Crystallogr B*, **1973**, *B 29*, 362-363.
- 12 du Boulay, D.; Maslen, E. N., *Acta Crystallogr B*, **1995**, *B 51*, 921-929.
- 13 Gibbs, A.S.; Knight, K.S.; Lightfoot, P., *Phys. Rev. B*, **2011**, *83*, 094111.
- 14 Marezio, M.; Dernier, P. D., *Mater. Res. Bull.*, **1971**, *6*, 23-29.
- 15 McCready, D. E.; Kingsley J. J., *Powder Diffr.*, **1994**, *9*, 143-145.
- 16 Vyshatko, N. P.; Kharton, V. V.; Shaula, A. L.; Marques, F. M. B., *Powder Diffr.*, **2003**, *18*, 159-161.
- 17 Howard, S. A.; Yau, J. K.; Anderson, H. U., *J. Appl. Phys.*, **1989**, *65*, 1492-1498.
- 18 Wang, Y.; Yu, L.; Wang, J. H.; Chen, L. W.; Gao, W. G.; Du, X. L.; Biao, L. H., *Mater. Lett.*, **2012**, *75*, 39-41.
- 19 Zeng, P. Y.; Ran, R.; Zhihao, C. A. H.; Zhou, W.; Gu, H. X.; Shao, Z. P.; Liu, S. M., *J. Alloys Compd.*, **2008**, *455*, 465-470.
- 20 Saito, S.; Nakahigashi, K.; Shimomura, Y., *J. Phys. Soc. Jpn.*, **1966**, *21*, 850-+.
- 21 Hanawalt, J. D.; Rinn, H. W.; Frevel, L. K., *Ind. Eng. Chem. Anal. Ed.*, **1938**, *10*, 457-512.
- 22 Stromme, K. O., *Acta Chem. Scand. A*, **1975**, *29*, 105-110.
- 23 Kuroda, K.; Ishizawa, N.; Mizutani, N.; Kato, M., *J. Solid State Chem.*, **1981**, *38*, 297-299.
- 24 Jacobson, A. J.; Hutchison, J. L., *J. Solid State Chem.*, **1980**, *35*, 334-340.
- 25 Liu, X.; Prewitt, C. T., *Phys. Chem. Miner.*, **1990**, *17*, 168-172.
- 26 Bell, A. M. T., *Supercond Sci Tech*, **1990**, *3*, 55-61.
- 27 Negas, T.; Roth, R. S., *J. Solid State Chem.*, **1971**, *3*, 323-339.
- 28 Liu, L. G., *J. Appl. Phys.*, **1971**, *42*, 3702.
- 29 McMurdie, H. F.; Golovato, E., *J Res Nat Bur Stand*, **1948**, *41*, 589-600.
- 30 Davey, W. P., *Phys. Rev.*, **1925**, *25*, 753-761.
- 31 Takeda, Y.; Kanno, R.; Takada, T.; Yamamoto, O.; Takano, M.; Bando, Y., *Z. Anorg. Allg. Chem.*, **1986**, *541*, 259-270.
- 32 Lehnert, H.; Boysen, H.; Schneider, J.; Frey, F.; Hohlwein, D.; Radaelli, P.; Ehrenberg, H., *Z. Kristallogr.*, **2000**, *215*, 536-541.
- 33 Spitsbergen, U., *Acta Crystallogr*, **1960**, *13*, 197-198.
- 34 Grenier, J. C.; Ghodbane, S.; Demazeau, G.; Pouchard, M.; Hagenmuller, P., *Mater. Res. Bull.*, **1979**, *14*, 831-839.
- 35 Barin, I., *Thermochemical Data of Pure Substances*, VCH Verlagsgesellschaft mbH, **1993**.